2008 IEEE International Conference on
Robotics and Automation
Pasadena, CA, USA, May 19-23, 2008

Maneuverability of a Robotic Tuna with Compliant Body

Anirban Mazumdar, Pablo Valdivia Y Alvarado*, and Kamal Youcef-Toumi Member IEEE

Abstract— **The maneuvering performance of a robotic device designed to mimic the swimming motions of Thunniform swimmers is presented. In contrast to existing designs, this design achieves fish like locomotion through the use of a single actuator and a compliant body and tail. Experiments were performed using both biased swimming motions and coasted turns. During these experiments the Compliant Robotic Tuna (CRT) achieved steady swimming speeds of up to 0.37 body lengths / second, average turning rates of up to 12.6 degrees per second, and turning radii as low as 1 body length. In addition, this paper compares the measured maneuvering performance with the predictions of a simplified rigid body model that was derived using both theoretical and empirical techniques. The swimming motions studied in this paper were achieved using open loop mechanisms. Therefore the potential for performance improvements exists.**

I. INTRODUCTION

Underwater robotic devices have many applications for both industry and defense. While such devices are already used for underwater exploration and pollution detection, many tasks and missions require devices that are highly maneuverable. In order to achieve improved maneuverability, numerous research efforts have focused on the area of biomimetic robotics. The goal of these efforts is to create unmanned undersea vehicles (UUV) that can achieve the swimming and maneuvering performance of fish. Tuna are an especially popular choice due to the fact that they are among the fastest swimmers [1]. In addition, tuna can achieve turning radii of 0.47 body lengths [2] which represents a significant improvement over conventional UUVs [3]. Such highly maneuverable vehicles could carry out missions in dangerous and harsh environments and therefore have direct relevance to many military and industrial applications. Robotic devices that emulate the swimming motion of biological organisms have been actively pursued throughout the past decade. For example, Triantafyllou and Barrett [5] designed the RoboTuna, and Liu and Hu have also developed a robotic fish [6]. In addition, Anderson and Chhabra used a robotic tuna to show that a biologically inspired UUV could provide significant improvements in maneuvering performance over conventional propeller driven UUVs [3].

For the most part, these designs employ classical mechanisms such as linkages and multiple actuators to recreate the complex swimming motions of fish like the tuna. However, recently Valdivia Y Alvarado and Youcef-Toumi produced a novel design involving the use of body compliance to achieve required body motions [7]. Due to its relative mechanical simplicity and efficiency, this new design holds promise as an alternative approach for the design of underwater vehicles. While the swimming dynamics and efficiency of such compliant biomimetic swimming devices has been studied [8], the maneuvering performance of such devices remains relatively unexplored. While this specific robotic device was designed for optimal forward motion (rather than turning motion), it is possible to use this methodology to design devices optimized for high maneuverability [9]. Therefore, it is still informative to study the maneuvering performance of a device with a compliant body based design. In this paper we present the experimental maneuvering results of the Mechatronics Research Laboratory's robotic tuna and compare them with the results of a simplified rigid body model. This robotic device was designed to specifically emulate the swimming motions of a thunniform swimmer like the tuna. Specifically, the robotic device uses the undulation of its body and caudal fin to create forward motion. This dynamic swimming motion is accomplished through the use of a single actuator in tandem with a compliant body. The tuna was chosen due the tuna's well-documented ability to swim at high speeds [1].

Specifically, two maneuvering behaviors are addressed in this paper. First, biased swimming motions were studied. Biased swimming motions consist of asymmetric tail oscillations. While symmetric tail oscillations should cause the Compliant Robotic Tuna (CRT) to swim straight, asymmetric motions should create turning motions. The second type of maneuvering behavior is the coasted turn. This type of turn involves the CRT swimming and then suddenly deflecting its tail and coasting into a turn. Both these maneuvering behaviors have utility. For example a coasted turn will achieve higher peak turning rates but requires that the CRT has already achieved a high forward velocity. In contrast, biased swimming allows the CRT to achieve turning motions from rest. Both of these maneuvering motions are modeled and studied in this paper.

II. ROBOTIC SYSTEM DESCRIPTION

The CRT used for the experiments outlined in this paper was designed and fabricated at the Mechatronics Research Laboratory (MRL) at the Massachusetts Institute of Technology (MIT) ([7], [8], [9]). The CRT is approximately 0.267 m long and possesses the characteristic Thunniform shape. The CRT itself is composed of silicon in a hybrid configuration. The prototype, as explained in [9], features

*Corresponding author: pablov@mit.edu
This work was partially funded by the Singapore MIT Alliance
A. Mazumdar is with the Department of Mechanical Engineering, Massachusetts Institute of Technology, amazumda@mit.edu
P. Valdivia Y Alvarado is with the Department of Mechanical Engineering, MIT pablov@mit.edu
K. Youcef-Toumi is on the faculty of the Department of Mechanical Engineering, MIT youcef@mit.edu

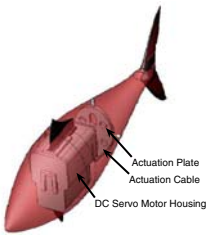

Fig. 1. The CRT system. The image shows the actuation components.

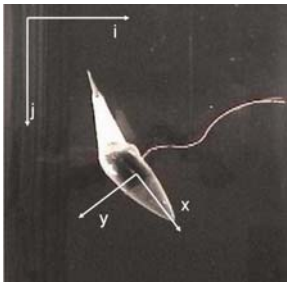

Fig. 2. The actual CRT system shown in the MRL tank during a coasted turn with tail deflection.

an anisotropic material distribution along its body length. These properties were carefully chosen to provide the desired swimming motions [9]. For propulsion the CRT contains a single DC Servo motor coupled with cables to an actuating plate (Fig. 1) [9]. This servomotor is used to actuate the tail. This feature represents a significant departure from other biomimetic robotic devices. For example, the robotic device presented by Liu and Hu employs 4 R/C servo motors to actuate the tail [6], while Anderson's Vorticity Controlled Unmanned Underwater Vehicle (VCUUV) makes use of a complex driven link assembly [3].

The CRT system is controlled using a robotics microcontroller board. The CRT system only requires a power supply and a pulse width modulation (PWM) signal. The servo motor applies a moment to the tail and the PWM signal is used to control the position of the tail. A set of tether wires provides the DC power and a PWM signal to the onboard servo motor. While an untethered and fully autonomous system has been created, the tethered device was used for this paper due to size constraints within the experimental setup

III. HYDRODYNAMIC MODEL

A. Equations of Motion

Rigid body dynamics were used to determine the motions of the center of mass while Lighthill's Elongated Body Theory [9] was used to account for the thrust created by the body undulations. While this is a somewhat simplistic approach that ignores some of the more complex dynamics, it enables the use of standard modeling and analysis techniques [3]. Therefore, this simplified model can provide physical intuition on a rather complex dynamic system. In this paper the standard naval architecture conventions (Society of Naval Architects and Marine Engineers, 1952) [10] are used.

A body centric coordinate system (this is a non inertial coordinate frame) was used with the x axis pointing along the body of the CRT (when straight) while the y axis points along the starboard direction and the z axis points downward [3]. The corresponding velocities are u (surge velocity) and v (sway velocity). The rotational velocity about the z axis is r (yaw). In addition, a fixed coordinate system was used to determine trajectories. The i and j directions lie in the xy plane and correspond to a fixed coordinate system centered at the edge of the tank. The j direction is parallel to the longitudinal direction of the tank while the i direction is perpendicular to it.

With the current design, the motion of the CRT is confined to the xy plane. Therefore, the equations of motions simplify considerably. The resulting equations of motion as outlined by Anderson in [3] and Triantafyllou in [4]are:

$$m\dot{u} = \sum F_x - m_{11}\dot{u} + m_{22}vr + m_{22}rr - mrv \quad (1)$$

$$m\dot{v} = \sum F_y - m_{22}\dot{v} - m_{26}\dot{r} - m_{11}ur + mru \quad (2)$$

$$I_{zz}\dot{r} = \sum M_z - m_{66}\dot{r} - m_{26}\dot{v} + (m_{11} - m_{22})uv - m_{26}ur \quad (3)$$

A dot above a variable is used to represent a time derivative. In these equations m represents the total mass while I_{zz} represents the moment of inertia about the z axis. The terms m_{ij} represent the terms of the added mass tensor. Lastly, F_x and F_y represent the external forces in the x and y directions while M_z represents the external moments about the z axis.

B. Hydrodynamic Coefficients

A simplified hydrodynamic model for the CRT was produced using a combination of analytic techniques and empirical results. The translational drag force was considered to be

$$F_{drag} = \frac{1}{2}\rho A k C_d U^2 \quad (4)$$

where C_d represents the net drag coefficient respectively, and k represents a correction factor. In addition, ρ represents the fluid density, A represents the appropriate area, and U represents the velocity along the particular direction.

Due to the complex geometry, unique shape, and the presence of control wires, it was difficult to determine the drag coefficient in the surge (x) direction using the standard tables such as those in Newman [11] and Hoerner [12]. Therefore, the static drag coefficients were estimated based on previous experimental data.

The drag coefficient in the sway (y) direction was determined by approximating the body as a flat plate and using the value found in Munson [13]. The fluid drag moment was approximated in a similar manner to that of Klaka [14]. The CRT was approximated as two flat plates of different lengths

TABLE I
SUMMARY OF HYDRODYNAMIC COEFFICIENTS

m (kg)	0.36
m_{11} (kg)	0.0555
m_{22} (kg)	0.4612
m_{66} (kgm^2)	$8.41 \cdot 10^{-4}$
m_{26} (kgm)	-0.0021
I_{zz} (kgm^2)	$7.53 \cdot 10^{-4}$
C_{dx} (wetted area)	0.15
C_{dy} (presented area)	1.9
C_{lift} (planform area)	0.5

and areas joined at the center of mass of the CRT. The drag moment was modeled as

$$M_{drag} = \frac{1}{2}\rho k C_{dy}((rD_1)^2 D_1 A_1 + (rD_2)^2 D_2 A_2) \quad (5)$$

where D_1 and D_2 represent the distance from the edges of the plates to the center of mass and A_1 and A_1 represent the areas of the upper and and lower portions of the plate respectively.

The correction factor k is based on the observation by Lighthill [18] that the measured drag coefficient and the predicted (based on geometry and Reynolds number) drag coefficient for a swimming fish differed by a factor of 4. Similarly, Smit [19] found that for fish, the swimming drag force exceeds the gliding drag force by a factor of roughly 3.6. Lighthill hypothesized that the swimming motions prevent the boundary layer from growing and therefore causes an increase in the skin friction along the surface of the fish.

It should be noted that this representation of the drag is hardly the only approach. While the fact that the dynamic drag exceeds the coasting drag has been observed experimentally by Anderson [16], the idea that thrust and drag are independent is still debated. For example, Schultz presents an approach based on inviscid Computational Fluid Dynamics [17] that predicts swimming speeds quite accurately. The reason the reduced order model was chosen was because it is the most physically intuitive and it also simplifies the modeling of both dynamic and steady (constant velocity) swimming.

The added mass tensor was computed using the methods outlined in [11]. Due to the fact that the shape of the CRT is irregular, strip theory was used to compute the added mass values. Due to the fact that the motion of the CRT is constrained to the xy plane, the only relevant added mass values were m_{11}, m_{22}, m_{66}, and m_{26}. These values along with the drag coefficients are summarized in Table 1.

C. Thrust Estimates

The thrust produced by the CRT was estimated using the Elongated Body Theory outlined by Sir James Lighthill [20]. Elongated Body Theory assumes inertial effects to be dominant and allows the use of an inviscid fluid model. While there certainly exist approaches that provide greater accuracy, the use of the Elongated Body Theory is relatively simple and physically intuitive [9]. Valdivia [9] showed that for a body lateral deflection described by,

$$h(x,t) = H(x)\sin(\omega t - \kappa x) \quad (6)$$

the average thrust can therefore be approximated as

$$\langle T \rangle = \frac{m(l)}{4}(H(l)^2(\omega^2 - \kappa^2 U^2) - U^2 H'(l)^2) \quad (7)$$

where H and H' represent the deflection and slope at the tip of the tail respectively. In addition, $m(l)$ represents the apparent mass at the tail, U represents the velocity, ω represents the angular frequency of the tail oscillation, and κ represents the wave number. The wave number can be calculated using the phase ϕ and the length l.

$$\kappa = \frac{\phi}{l} \quad (8)$$

The thrust estimate can be decomposed into the x and y directions using the tail angle. For biased swimming motions, the term tail angle corresponds to the average angle of the tail with respect to trajectory of the CRT (a perfectly symmetric swimming motion would result in a tail angle of 0 degrees)(Fig. 3). For a more detailed explanation refer to [9].

D. Tail Deflection Estimates

As illustrated above, the thrust calculations are heavily dependent on the tail deflection. The current version of the CRT has no internal sensors to measure the tail deflection. Therefore, in order to estimate the thrust, the tail deflection and phase must be approximated. In [9] Valdivia showed that

$$H \sim \frac{\frac{M}{(l-a)^2}}{\sqrt{(\frac{EI}{(l-a)^2} - (\rho A + m(l))\omega^2)^2 + (\frac{\mu I \omega}{(l-a)^4})^2}} \quad (9)$$

$$\phi \sim \arctan\left(\frac{\frac{\mu I \omega}{(l-a)^4}}{\frac{EI}{(l-a)^4} - (\rho A + m(l))\omega^2}\right) \quad (10)$$

where M represents the input moment, l represents the length of the body, a represents the distance from the head to the actuation location, ω represents the angular frequency. Similarly, E, μ, and ρ represent the modulus of elasticity, viscosity, and density of the tail material. Finally, I, A, $m(l)$ represent the second moment of inertia, cross sectional area, and added mass of the tail respectively. From this equation it is clear that the deflection is directly dependent on the applied moment M while all other properties are physical properties of the CRT. For a more detailed explanation refer to [9].

E. Dynamic Simulations

A set of dynamic simulations were developed to properly asses the dynamic model. These simulations were based on equations (1-9) which combine to provide

$$
\begin{aligned}
m\dot{u} &= -m_{11}\dot{u} + m_{22}vr + m_{22}rr - mrv - F_{dragX} \\
&\quad + \langle T \rangle \cos\theta \qquad (11) \\
m\dot{v} &= -m_{22}\dot{v} - m_{26}\dot{r} - m_{11}ur + mru - F_{dragY} \\
&\quad + \langle T \rangle \sin\theta \qquad (12) \\
I_{zz}\dot{r} &= -m_{66}\dot{r} - m_{26}\dot{v} + (m_{11} - m_{22})uv \\
&\quad - m_{26}ur - \langle T \rangle l_{tail} \sin\theta - M_{drag} - M_{dragY} \qquad (13)
\end{aligned}
$$

where θ represents the average tail angle, l_{tail} represents the moment arm for the tail and M_{dragY} represents the drag moment from motions in the y direction. The equations of motion were solved iteratively in Matlab Simulink. Two separate simulations were designed to match each type of maneuvering motion (biased turning and coasted turning).

There were some changes made to the simulation for the coasted turn. The CRT only experiences a short thrust input at the instant of the coast turn. In addition the drag coefficients were adjusted to account for the fact that during a coasted turn the CRT is no longer swimming and therefore should no longer experience boundary layer thinning. Other changes included the addition of drag forces and moments to account for the deflection of the entire tail. Finally it was assumed that the tail deflection acts in a manner similar to a rudder. Therefore, the lift force for such a rudder was calculated by approximating the tail as a flat plate and using the equations outlined in [4]. The lift coefficient from [21] for the rudder is provided in Table 1.

IV. EXPERIMENTAL SETUP

A. Goals

The purpose of these experiments was to measure the maneuvering performance of the CRT. Specifically, values for the turning radius, average turning rate, and forward swimming velocity were desired. In order to achieve these measurements, two different experiments were performed. The first set of experiments focused on biased swimming motions and involved allowing the CRT to begin at rest and then sending a signal to begin forward swimming. All experiments took place at the same swimming frequency of 2Hz. The 2 Hz frequency was chosen because it provides near peak swimming performance for the device. For each trial the CRT was filmed as it transitioned from rest to steady motion.

The second set of experiments involved studying a coasted turn. The CRT was initially allowed to swim straight and achieve steady swimming. Once steady motion was achieved, the CRT was sent a signal corresponding maximum tail deflection and allowed to coast to a stop (Fig. 2). It should be noted that the entire body and tail of the CRT deflect.

B. Experimental Apparatus

The experiments were performed in the MRL tank at MIT. The MRL tank is a 2.5m by 0.6m by 0.6m acrylic tank. The tank is large enough for the CRT to achieve steady motions from rest initial conditions. A Sony DCR-TRV30 NTSC MiniDV digital camera was used to film the experiments. The experimental setup also included the CRT system described above and a PlugaPod Microcontroller board with a custom program was used to provide the PWM signals corresponding to the desired swimming behavior [8].

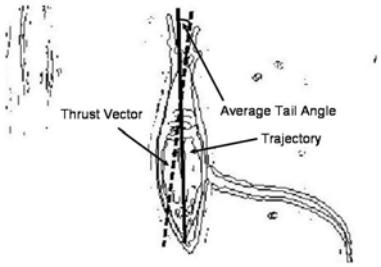

Fig. 3. An illustration of the average tail angle and the thrust vector. This image shows both the maximum and minimum tail positions overlayed upon each other. Note how the estimated tail thrust direction is not parallel with the trajectory.

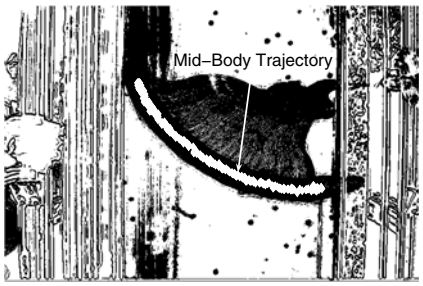

Fig. 4. The output of the matlab video processing program. The trajectory of the midbody of the CRT is labeled with white diamonds.

C. Data Analysis

The experimental data was analyzed using a custom written video analysis Matlab program that assessed the configuration of the CRT at each frame. Results of this program can be seen in Fig. 4. This program computed the x and y trajectories of the CRT and used a polynomial fit to determine the total distance traveled along the trajectory. From this information the velocity of the CRT was approximated. The orientation of the swimming device was measured by creating a line between the nose and mid body. The angle created by this line and the j axis was assumed to be the orientation of the CRT. The tail angle was measured in a similar manner. In order to obtain a single value for the turning radius, circular turning trajectories were assumed. The radius of this circle was approximated by dividing the total distance traveled by the net change in orientation.

D. Results

1) Biased Turning Results: For the biased turns, a number of experiments were performed with average tail angle

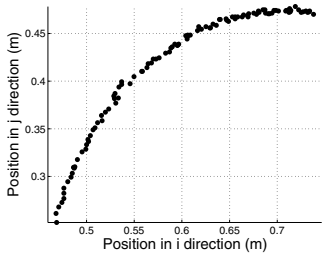

Fig. 5. A graphical representation of the measured biased turning trajectory.

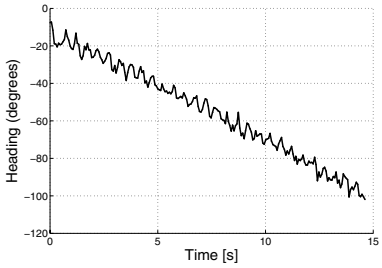

Fig. 6. A graphical representation of the measured orientation during a biased turn. Note the oscillatory nature of the angle. This is due to the body and head oscillations that occur during the swimmming motion.

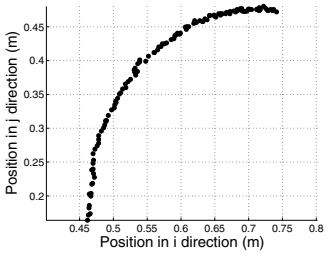

Fig. 7. A graphical representation of the measured coasted turning trajectory. Note the initially straight trajectory that corresponds to steady swimming before the turn command.

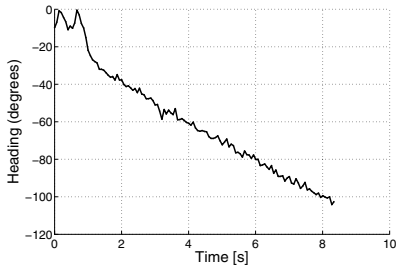

Fig. 8. A graphical representation of the measured orientation during a coasted turn. Note the oscillatory nature of the angle before t = 1s and the subsequent rapid change in orientation.

ranging from approximately 3 degrees to 12.5 degrees. Peak turning occurred with an average tail angle of 12.5 degrees. Fig. 5 illustrates the trajectory of the CRT with regard to the fixed coordinate frame of the tank, while Fig. 6 shows the orientation of the CRT through the turn.

In the past similar studies [3] have used the turning radius and the average turning rate as the metrics for maneuverability. For these studies, the average turning rates ranged from 0.27 degrees/s to 6.1 degrees/s and the turning radius ranged from 15 body lengths to 1.2 body lengths. For the sake of comparison, the conventional UUV studied by Anderson, achieved an average turning rate of 4 degrees/s and a turning radius of 2.7 body lengths, while Anderson's biomimetic VCUUV achieved a turning radius of 0.5 body lengths.

The steady swimming velocities in the x direction were also measured. These velocities ranged from 0.203 body lengths per second (BL/s) to 0.34 BL/s. This illustrates that during a biased turning motion, the CRT can still maintain a net velocity that is approximately 55 percent of the maximum velocity rather than being forced to slow to a stop.

2) Coasted Turn Results: For the coasted turn, the CRT was allowed to swim straight until it achieved a steady swimming velocity of approximately 0.37 BL/s or 0.1 m/s. The CRT was then sent a signal for maximum tail deflection and was allowed to coast. The measured deflection tail angle was 23 degrees. This value represents the maximum achievable tail static tail deflection. Fig. 7 provides a graphical representation of the coasted turning trajectory.

At this tail angle, the CRT turned 94 degrees in 7.47 seconds (Fig. 8). This corresponds to an average turning rate of 12.6 degrees/s. In addition, the turning radius was measured to be approximately 1.0 body lengths. Lastly, through the coasted turn, the CRT achieved a peak turning rate of approximately 28 degrees/s. Performing a similar maneuver, Anderson's biomimetic VCUUV achieved a peak turning rate of 75 degrees /s, and an average turning rate of approximately 16 degrees/s [3].

V. DISCUSSION

An examination of the data provided in Fig. 9 and Fig. 10 reveals that the performance at low tail angles appears highly erratic. In fact, at certain angles the measured data illustrates a positive yaw rate instead of the negative rate predicted by the model. A likely explanation for this is that at small tail angles the turning torque from the tail does not dominate. Therefore, other factors such as asymmetric surface finish and the presence of control wires can contribute. With this observation, the data appears more logical. For angles above 3 degrees, the measured data matches the overall trend predicted by the model.

Unfortunately, there exist significant errors between the measured and predicted results for the turning radius. Even at high tail angles, the errors are on the order of 50 percent. A likely explanation is that the thrust-drag predictions in the x (surge) direction are not correct. This explanation is supported by the fact that the model predicts a significantly higher steady swimming speed (0.43 BL/s) than the measured value (0.34 BL/s). While these errors are on the order of 25 percent, the velocity errors propagate due to the integration used to find total distance traveled. The 25 percent error in the velocity prediction is in fact somewhat expected.

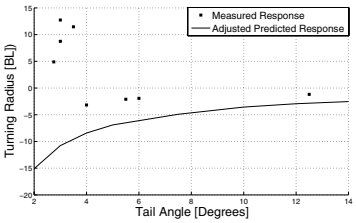

Fig. 9. A comparison of the predicted and measured turning radii for various tail angles. While turning radius cannot technically be negative, the sign is used to differentiate between turning directions.

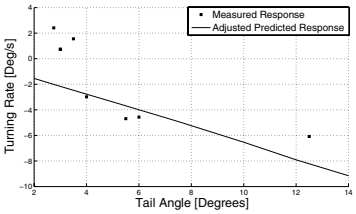

Fig. 10. A comparison of the predicted and measured turning rates for various tail angles

Drag coefficients and the scaling factor used to account for boundary layer thinning are hardly exact or precise. In addition, it was shown by Cheng [22] that Lighthill's Elongated Body Theory can overpredict the thrust.

Similarly, for the coasted turn, the measured results roughly match the predictions of the model. The adjusted model predicted a turning rate of 9.42 degrees per second and a turning radius of 1.03 body lengths. Therefore, the model had errors of 25 percent and 3 percent for the turning rate and turning radius respectively.

VI. SUMMARY

This paper has presented the maneuvering performance of an underwater vehicle that uses a compliant mechanism to achieve biomimetic behavior. The maneuvering performance exceeds that of the conventional UUV presented by Anderson but does not match Anderson's VCUUV. It should be noted that the CRT was not originally designed to optimize turning and maneuvering. In addition this performance was achieved using open loop systems, and the use of closed loop controls could significantly improve maneuvering performance.

During experimental trials the CRT achieved velocities of 0.1 m/s or 0.37 BL/s. In addition, using biased swimming motions, the CRT achieved an average turning rate of 6.1 degrees/s with a turning radius of 1.18 body lengths. Similarly during a coasted turn the CRT achieved an average turning rate of 12.6 degrees/s and a turning radius of 1 body length.

A simplified model was also outlined in this paper, and relevant drag coefficients and added mass values were estimated. The body of the CRT was approximated as a rigid body with an undulating tail, and Lighthill's Elongated Body Theory was used to estimate the thrust from the tail deflection. Since the actual swimming dynamics are highly complex the goal of this model was to provide intuition into the maneuvering behavior of the CRT. In this regard the simplified model is a valuable first step into further understanding these devices.

This paper also reveals areas of future work. Clearly a closed loop system to control the tail deflection of the CRT is essential for further experiments and applications. In addition, now that the maneuverability has been illustrated a logical extension is to implement heading control and trajectory tracking controls.

REFERENCES

[1] J.E. Colgate, and K.M. Lynch. 2004. Mechanics and Control of Swimming: A Review. IEEE Journal of Oceanic Engineering. 29:660-673.

[2] R.W. Blake, L. M. Chatters, and P. Domenici. 1995. Turning radius of yellowfin tuna (*Thunnus albacares*) in unsteady swimming manoevres. J. Fish Biol. 46:536-538.

[3] J. M. Anderson, and N.K. Chhabra. 2001. "Maneuvering and Stability Performance of a Robotic Tuna", *Proc. Meeting of the Society for Integrative and Comparative Biology*, Chicago Illinois, 2001.

[4] M.S. Triantafyllou and F.S. Hover. 2003. Maneuvering and Control of Marine Vehicles.

[5] D. Barrett. 1996. Propulsive efficiency of a flexible hull underwater vehicle, Ph.D. Diss., Massachusetts Institute of Technology, Cambridge, Massachusetts.

[6] J. Liu and H. Hu. 2005. "Mimicry of Sharp Turning Behaviours in a Robotic Fish", *Proc. International Conference on Robotics and Automation*, Barcelona Spain, April, 2005.

[7] P. Valdivia, Y Alvarado, and K. Youcef-Toumi. 2006. Design of Machines with Compliant Bodies for Biomimetic Locomotion in Liquid Environments. Journal of Dynamic Systems, Measurement, and Control.

[8] P. Valdivia, Y Alvarado, and K. Youcef-Toumi. 2005. Performance of Machines with Compliant Bodies Designed for Biomimetic Locomotion in Liquid Environments. *Proc. International Conference on Robotics and Automation*, Barcelona Spain, April, 2005.

[9] P. Valdivia Y Alvarado. Design of Biomimetic Compliant Devices for Locomotion in Liquid Environments, Ph.D. Diss., Department of Mechanical Engineering, Massachusetts Institute of Technology, Cambridge, Massachusetts.

[10] Society of Naval Architects and Marine Engineers. 1952. Nomenclature for treating the motion of a submerged body through fluid, SNAME Technical and Research Bulletin No. 1-5, April, 1952.

[11] J.N. Newman. 1977. Marine Hydrodynamics. MIT Press, Cambridge, Massachusetts.

[12] S. Hoerner. 1965. Fluid-Dynamic Drag. Hoerner Fluid Dynamics, Vancouver, WA. pp 3-1 to 3-28.

[13] B.R. Munson, D.F. Young, T.H. Okiishi. 1998. Fundamentals of Fluid Mechanics. John Wiley and Sons, New York.

[14] K. Klaka. 2003. Hydrodynamic tests on a flat plate in forced oscillation. Internal Report. Centre for Marine Science and Technology, Curtin University of Technology, Perth, Australia.

[15] F.E. Fish, and G.V, Lauder. 2006. "Passive and Active Flow Control by Swimming Fishes and Mammals". A. Rev. Fluid Mech., 38. pp 193-224.

[16] E.J. Anderson, W. R. McGillis, and M. A. Grosenbaugh. 2001. The boundary layer of swimming fish. J. Exp. Bio. 204:81-102.

[17] W.W. Schultz, and P. W. Webb. 2002. Power Requirements of Swimming: Do New Methods Resolve Old Questions?. Integr. Comp. Biol., 42: 1018:1025.

[18] J. Lighthill. 1975. Mathematical Biofluiddynamics. Society for Industrial and Applied Mathematics, Philadelphia Pennsylvania. pp 112.

[19] H. Smit. 1965. Can. J. Zool. 43, 632.

[20] J. Lighthill. 1960. "Note on the Swimming of Slender Fish". A. Rev. Fluid Mech., 9. pp 112-113.

[21] J.D. Anderson. 1999. A History of Aerodynamics. Cambridge University Press, Cambridge, United Kingdom.

[22] J. Cheng, L. Zhuang, B. Tong. 1991 Analysis of swimming of three-dimensional waving plates. J. Fluid Mech. 232, 341-355.